XBP1s activation can globally remodel N-glycan structure distribution patterns

Madeline Y. Wong[a,1], Kenny Chen[a,1], Aristotelis Antonopoulos[b,1], Brian T. Kasper[c,1], Mahender B. Dewal[a,2], Rebecca J. Taylor[a,3], Charles A. Whittaker[d], Pyae P. Hein[a,4], Anne Dell[b], Joseph C. Genereux[e], Stuart M. Haslam[b,5], Lara K. Mahal[c,5], and Matthew D. Shoulders[a,5]

[a]Department of Chemistry, Massachusetts Institute of Technology, Cambridge, MA 02139; [b]Department of Life Sciences, Imperial College London, London SW7 2AZ, United Kingdom; [c]Biomedical Chemistry Institute, Department of Chemistry, New York University, New York, NY 10003; [d]Barbara K. Ostrom (1978) Bioinformatics and Computing Facility, Massachusetts Institute of Technology, Cambridge, MA 02139; and [e]Department of Chemistry, University of California, Riverside, CA 92521

Edited by Chi-Huey Wong, Academia Sinica, Taipei, Taiwan, and approved September 14, 2018 (received for review April 12, 2018)

Classically, the unfolded protein response (UPR) safeguards secretory pathway proteostasis. The most ancient arm of the UPR, the IRE1-activated spliced X-box binding protein 1 (XBP1s)-mediated response, has roles in secretory pathway maturation beyond resolving proteostatic stress. Understanding the consequences of XBP1s activation for cellular processes is critical for elucidating mechanistic connections between XBP1s and development, immunity, and disease. Here, we show that a key functional output of XBP1s activation is a cell type-dependent shift in the distribution of N-glycan structures on endogenous membrane and secreted proteomes. For example, XBP1s activity decreased levels of sialylation and bisecting GlcNAc in the HEK293 membrane proteome and secretome, while substantially increasing the population of oligomannose N-glycans only in the secretome. In HeLa cell membranes, stress-independent XBP1s activation increased the population of high-mannose and tetraantennary N-glycans, and also enhanced core fucosylation. mRNA profiling experiments suggest that XBP1s-mediated remodeling of the N-glycome is, at least in part, a consequence of coordinated transcriptional resculpting of N-glycan maturation pathways by XBP1s. The discovery of XBP1s-induced N-glycan structural remodeling on a glycome-wide scale suggests that XBP1s can act as a master regulator of N-glycan maturation. Moreover, because the sugars on cell-surface proteins or on proteins secreted from an XBP1s-activated cell can be molecularly distinct from those of an unactivated cell, these findings reveal a potential new mechanism for translating intracellular stress signaling into altered interactions with the extracellular environment.

N-glycosylation | proteostasis | glycoproteome | lectin microarray | endoplasmic reticulum

The unfolded protein response (UPR) is classically responsible for maintaining proteostasis in the secretory pathway (1). In the metazoan UPR, three transmembrane proteins (IRE1, PERK, and ATF6) act to detect protein misfolding stress in the endoplasmic reticulum (ER). Once stress is detected, activation of each sensor results in the production of a distinctive transcription factor—spliced X-box binding protein 1 (XBP1s), ATF4, or ATF6(1–373), respectively (2). The targets of these transcription factors include a suite of ER chaperones and quality control factors that can resolve proteostatic challenges caused by physiologic and environmental changes. The central role of the UPR in maintaining secretory proteostasis has catalyzed extensive efforts to delineate relevant mechanisms of induction (3), define cellular effects of UPR activation, and create tools to modulate individual UPR arms (4–6).

The IRE1-XBP1s pathway is the most ancient UPR arm (2). Recent work continues to define essential functions for the XBP1s transcription factor, in particular, that are distinctive from proteostasis maintenance. For example, XBP1s is critical for development, immune response, memory formation, and cell-nonautonomous ER stress signaling (7–10). Moreover, chronic up-regulation of the XBP1s transcription factor is a pathologic hallmark of numerous malignancies (11). Consistent with its diverse regulatory functions, the IRE1-XBP1s arm can be activated independent of PERK-ATF4 and ATF6 in response to assorted stimuli (1). Attaining mechanistic understanding of these diverse processes requires first comprehensively defining the molecular consequences of XBP1s induction.

The majority of proteins traversing the secretory pathway are co- or posttranslationally N-glycosylated (12). A 14-residue oligosaccharide with the structure $Glc_3Man_9GlcNAc_2$ (Glc, glucose; Man, mannose; GlcNAc, *N*-acetylglucosamine) is installed on Asn residues within specific amino acid sequons. XBP1s may modulate the extent to which N-linked glycans are installed by the cell (13), thereby potentially assisting N-glycoprotein trafficking and directly enhancing proteostasis by providing improved access to the ER's

Significance

Diverse polysaccharides are installed on specific asparagine residues as glycoproteins traverse the endoplasmic reticulum and Golgi. These N-glycan structures comprise the N-glycome, which coats cell surfaces, regulates cell–cell and cell–matrix interactions, and has functional consequences for immune system function and beyond. Our understanding of how intracellular signaling regulates the molecular architecture of the N-glycome remains immature. We show that the transcription factor XBP1s alters N-glycan structures displayed on endogenous membrane-associated and secreted glycoproteins, coincident with XBP1s-induced changes in N-glycosylation–related transcripts. These results establish a role for the unfolded protein response in defining the global composition of the N-glycome–providing a mechanism for transducing internal stress to an external signal, a phenomenon with implications for both normal biology and pathology.

Author contributions: M.D.S. conceived research; M.Y.W., K.C., M.B.D., A.D., S.M.H., L.K.M., and M.D.S. designed experiments; M.Y.W., K.C., A.A., B.T.K., M.B.D., R.J.T., P.P.H., and J.C.G. performed research; M.Y.W., K.C., A.A., B.T.K., C.A.W., A.D., J.C.G., S.M.H., L.K.M., and M.D.S. analyzed data; and M.Y.W., K.C., A.A., B.T.K., C.A.W., A.D., J.C.G., S.M.H., L.K.M., and M.D.S. wrote the paper.

The authors declare no conflict of interest.

This article is a PNAS Direct Submission.

Data deposition: The RNA-sequencing analysis reported in this paper has been deposited in the Gene Expression Omnibus (GEO) database, https://www.ncbi.nlm.nih.gov/geo/ (accession no. GSE112589).

[1]M.Y.W., K.C., A.A., and B.T.K. contributed equally to this work.

[2]Present address: Expansion Technologies, Inc., Cambridge, MA 02139.

[3]Present address: Department of Chemistry and Chemical Biology, Harvard University, Cambridge, MA 02138.

[4]Present address: Molecular Biology, Takeda Pharmaceuticals, Inc., Cambridge, MA 02139.

[5]To whom correspondence may be addressed. Email: s.haslam@imperial.ac.uk, lkmahal@nyu.edu, or mshoulde@mit.edu.

This article contains supporting information online at www.pnas.org/lookup/suppl/doi:10.1073/pnas.1805425115/-/DCSupplemental.

Published online October 10, 2018.

lectin-based chaperone and quality control machineries. Downstream of N-glycan installation, the immature sugar is processed in both the ER and the Golgi to yield the vast array of high- and oligomannose, hybrid, and complex N-glycan structures presented on secreted and cell-surface proteins (14). The molecular architecture of this N-glycome is dynamic, with consequences for both normal and pathologic processes, including cell motility and adhesion, cell–cell interactions, and immune system function (15–17). However, our understanding of how intracellular signaling pathways coordinately define N-glycan maturation and thereby regulate these processes remains incomplete.

We previously reported that stress-independent activation of XBP1s can significantly modify the structural distribution of N-glycans installed at the single N-glycosylation site of a soluble, secreted glycoprotein domain derived from the CD2 adhesion protein (18). The observed changes were specifically caused by XBP1s-mediated alterations in N-glycan maturation, not by modified CD2 protein synthesis or trafficking. These findings hint at the possibility that XBP1s may regulate the molecular architecture of the endogenous N-glycome in a coordinated manner. However, the CD2 protein domain used in our prior studies was an ectopically expressed, soluble, and glycosylation-naïve protein variant (18), rendering the biological relevance of the observed XBP1s-dependent remodeling of N-glycan maturation uncertain.

Here, we ask (*i*) whether induction of the transcription factor XBP1s results in altered N-glycan structures on endogenous proteins, and (*ii*) whether such remodeling is sufficiently significant to be observed in a glycome-wide experiment, not just on individual, purified glycoproteins. We find that stress-independent XBP1s activation can substantially alter the composition of the N-glycome in a cell type- and proteome-dependent manner. The resulting changes in the distribution of N-glycan structures indicate that XBP1s-activated cell membranes, and proteins secreted from XBP1s-activated cells, are often distinguishable at the molecular level from those of cells with basal levels of UPR signaling. These observations suggest a new mechanism to translate intracellular stress signaling to the extracellular milieu, a phenomenon with important implications for our emerging understanding of how the UPR shapes higher-order biological activities (e.g., organismal development and immune response) beyond just the maintenance of ER proteostasis.

Results

Experimental Platform and Workflow to Scrutinize Effects of XBP1s on the N-Glycome. Our objective here was to test the hypotheses that XBP1s-mediated remodeling of N-glycan structures (*i*) occurs on endogenous glycoproteins and (*ii*) is sufficiently significant to be observed in experiments surveying the glycome. Application of a traditional ER stress inducer such as thapsigargin (Tg) does cause XBP1s activation, and is therefore one possible experimental approach. However, the pleiotropic consequences of ER stressors, including extensive ER protein misfolding and high cytotoxicity, limit the reliability and interpretation of the resulting data. Selective induction of XBP1s using chemical genetics is an alternative strategy that we and others have employed to elucidate consequences of XBP1s activity (4, 19). This strategy results in XBP1s induction in the absence of global UPR activation by ER stress. Such selective and chronic XBP1s activation is observed in numerous relevant settings, including development, the immune response, and cancer (7, 8, 11).

In this work, we employed two cell lines engineered for ER stress-independent induction of XBP1s transcriptional activity. In both cell lines, XBP1s was placed under control of the tetracycline repressor, providing doxycycline (dox)-regulated expression of XBP1s. The first stable cell line we used, termed HEK^{XBP1s}, was derived from the human embryonic kidney cell line and was reported previously (4). The second cell line, developed for this study, was a stable HeLa cell line (derived from the cervical epithelial line) termed HeLa^{XBP1s}. In both HEK^{XBP1s} (*SI Appendix*, Fig. S1*A*) and HeLa^{XBP1s} (*SI Appendix*, Fig. S1*B*) cells, treatment with dox up-regulated mRNA expression for the established XBP1s target genes *ERDJ4* and *SEC24D* to levels similar to those induced by treatment with the classic ER stressor Tg. In both cases, XBP1s activation occurred independent of global UPR induction, as well-known transcripts induced by the PERK-ATF4 arm of the UPR were not up-regulated (e.g., *CHOP* and *GADD34*; *SI Appendix*, Fig. S1 *A* and *B*).

In previous work, we characterized the consequences of sustained XBP1s activation for the transcriptome and proteome of HEK^{XBP1s} cells (4). As the HeLa^{XBP1s} cell line was newly developed, we sequenced mRNA from vehicle-, dox-, or Tg-treated HeLa^{XBP1s} cells in biological triplicate. Hierarchical clustering of differentially expressed coding genes showed that XBP1s activation preferentially clustered with vehicle-treated rather than Tg-treated samples, indicating that the transcriptional consequences of chronic XBP1s activation were significantly muted relative to treatment with an ER stressor (*SI Appendix*, Fig. S1*C*). As expected (*SI Appendix*, Fig. S1*D*), and in line with our previous observations for HEK^{XBP1s} cells (4), gene set enrichment analysis revealed specific gene sets enriched in the XBP1s-activated lines alone (e.g., the unfolded protein binding gene set), others that were enriched in both XBP1s-activated and Tg-treated cells (e.g., the response to ER stress gene set), and a third group of gene sets enriched only in Tg-treated cells (e.g., the intrinsic apoptotic signaling in response to the ER stress gene set) (see Dataset S1 *A–D* for full results). HEK^{XBP1s} and HeLa^{XBP1s} cells thus provide two distinct cell types in which we can induce sustained XBP1s activity over the time period required for an intracellular signal like XBP1s-mediated transcription to propagate to the mature N-glycoproteome.

With appropriate cell lines in hand, we devised an experimental workflow to test for effects of XBP1s activation on N-glycan maturation. As illustrated in Fig. 1*A*, we treated HEK^{XBP1s} cells in complete media with vehicle (control), dox (to activate XBP1s), or Tg (to induce ER stress and the global UPR), followed by isolation of the membrane fraction by ultracentrifugation. Alternatively, we treated HEK^{XBP1s} cells identically in a serum-free media formulation (FreeStyle media) such that we could harvest and concentrate the secreted proteome for downstream glycomic analyses while minimizing contamination from serum glycoproteins. We used FreeStyle media instead of serum-free Dulbecco's modified Eagle's medium (DMEM) because we have observed that serum-free DMEM causes significant cell stress over longer treatments such as the 24 h used here. Grp78 was detected in the FreeStyle media only upon XBP1s activation (*SI Appendix*, Fig. S2), suggesting that the presence of any ER proteins in the XBP1s-activated secretome is a consequence of UPR activity, as has previously been observed by others (20). For HeLa^{XBP1s} cells, we carried out an identical workflow but isolated only the membrane fraction, as in our observation HeLa cells are less secretory than HEK cells.

After isolating membrane and secreted protein fractions, we next carried out two types of glycomic experiments on the samples: (*i*) lectin microarray analysis, which enabled us to directly compare relative levels of glycan motifs/substructures (21), and (*ii*) mass spectrometry, which provided a more detailed analysis of glycan structures. We used dual-color lectin microarrays (Fig. 1*B*) on biological triplicates to gain insight into potential glycome remodeling owing to XBP1s activation and/or Tg treatment. We measured the relative binding of fluorescently labeled glycoproteome samples and an orthogonally labeled common reference to immobilized lectins on our microarray. The lectin microarrays we employed were composed of ∼90 unique lectins with diverse sugar-binding specificities (see Dataset S2 for a complete list). Samples were labeled with Alexa Fluor 647 or 555, mixed with an equal amount of an orthogonally labeled common reference sample (a mix of all replicates for all conditions), and incubated with the microarray. The resulting data leverage the known glycan-binding preferences of lectins to gain insight into changes in the levels of glycan substructures, providing a systems-level perspective on differences in glycan epitopes via relative quantitation of the glycan epitopes/substructures recognized by a particular lectin across sample conditions (21).

We also used MALDI-TOF MS and TOF/TOF MS/MS (Fig. 1*C*) to obtain a molecular-level view of N-glycome composition in our samples. We performed GC-MS linkage analyses in parallel,

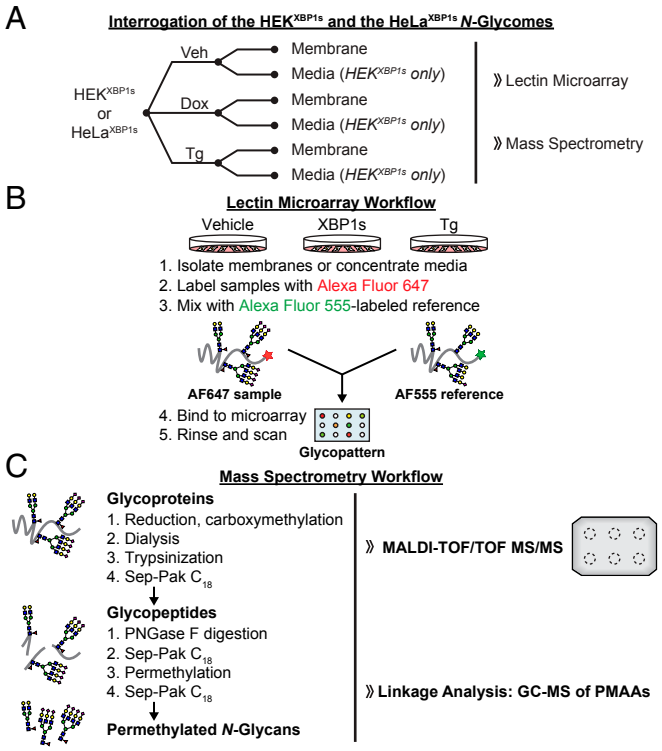

Fig. 1. Experimental workflows for glycomic analyses. (*A*) Experimental workflow for glycoproteome extraction and analysis. (*B*) Glycan analysis by lectin microarrays. (*C*) MS analysis of N-glycomes.

yielding further detail by characterizing specific sugar linkages. All MS analyses were performed in a minimum of biological duplicate. These MS techniques provide detailed structural information to validate and enhance the lectin microarray findings. Notably, while MS can pinpoint shifts in the overall composition of the glycome within a sample (i.e., what percentage of overall glycans in a given sample have sialic acid), the methods used here do not provide direct comparison of a specific glycan's absolute abundance between two samples (e.g., how much sialic acid is expressed in sample 1 vs. sample 2). Thus, percentage changes from MS represent shifts in the profile whereas percentage changes from the lectin microarray represent changes in the overall levels of an epitope. By combining the ability of lectin microarrays to provide collective expression changes for glycan motifs (regardless of parent glycan backbone) with the capacity of MS to supply detailed structural analysis of individual glycans, we were able to evaluate at high resolution whether and to what extent XBP1s modulates glycome architecture. Results from these complementary analyses are presented below.

XBP1s Remodels the HEK^{XBP1s} Cell-Membrane N-Glycome. We began by assaying the N-glycome of HEK^{XBP1s} cell membranes upon XBP1s activation or Tg treatment, following the workflow in Fig. 1*A*. Lectin microarray analysis of selective XBP1s activation in HEK^{XBP1s} membranes (Dataset S3*A*) revealed a significant decrease in α2,6-sialylation (Fig. 2*A* and *SI Appendix*, Fig. S3*A*, *Left*). The α2,6-sialic acid-specific lectins SNA-I, TJA-I, and PSL-I showed an average 29% decrease in binding relative to the vehicle-treated control. Our engineered recombinant lectin diCBM40, which binds both α2,3- and α2,6-linked sialic acids with similar affinity (22), showed a 35% loss in binding, further supporting a decrease in α2,6-sialylation. XBP1s activation also decreased bisecting N-glycans, as indicated by decreasing PHA-E signal (Fig. 2*A* and *SI Appendix*, Fig. S3*A*, *Left*).

Fully consistent with the lectin microarray analyses, MALDI-TOF MS analysis confirmed that XBP1s activation of HEK^{XBP1s} cells resulted in reduced sialylation of cell-membrane N-glycans and provided additional detail to the specific epitopes affected. Specifically, in XBP1s-activated cells, the relative abundance of ions at *m/z* 3054 and 3415 (green peaks in Fig. 2*B*, *Top* versus Fig. 2*B*, *Middle*)—corresponding to triantennary N-glycans with one or two NeuAc (*N*-acetylneuraminic acid) residues, respectively—decreased substantially (e.g., ∼84% for *m/z* 3054) with respect to the relative abundance of the ion at *m/z* 2693, an undecorated triantennary N-glycan. Similar results were observed for tetraantennary N-glycans in XBP1s-activated cells (red peaks in Fig. 2*B*, *Top* versus Fig. 2*B*, *Middle*). Specifically, the relative abundance of ions at *m/z* 3503, 3864, and 4226, which correspond to singly, doubly, and triply sialylated structures, decreased substantially (e.g., ∼85% for *m/z* 3503) upon XBP1s activation compared with the relative abundance of the undecorated tetraantennary N-glycan at *m/z* 3142. Similar but less intense reductions in sialylation were also observed for higher-mass N-glycans (*SI Appendix*, Fig. S3*B*). For example, in XBP1s-activated cells, the ions at *m/z* 5124 and 5485—corresponding mainly to tetraantennary N-glycans with two additional LacNAc (*N*-acetyllactosamine) repeats and three or four NeuAc residues—decreased by ∼22 and ∼44%, respectively, compared with the relative abundance of the ion at *m/z* 4763, which only has two NeuAc residues (*SI Appendix*, Fig. S3*B*, *Top* versus *SI Appendix*, Fig. S3*B*, *Middle*). Lower-mass biantennary glycans also displayed an ∼80% decrease in sialylation (*SI Appendix*, Fig. S3*C*, *Left* versus *SI Appendix*, Fig. S3*C*, *Middle*).

We also performed GC-MS analysis (*SI Appendix*, Table S1) to add linkage details to our findings from the MALDI-TOF MS, and to further evaluate our lectin microarray findings. The detection of 6-linked galactose showed that a portion of NeuAc residues were α2,6-linked. The abundance of these α2,6-linked NeuAc residues substantially decreased in XBP1s-activated HEK^{XBP1s} cells (23.6% in vehicle samples versus 4.0% in XBP1s-activated samples), in concordance with the lectin microarray data that specifically indicated reduced α2,6-sialylation (Fig. 2*A*). We also identified 3,4,6-linked mannose by GC-MS, verifying the presence of minor amounts of bisecting N-glycans in HEK^{XBP1s} cell membranes. The abundance of these epitopes also decreased upon XBP1s activation in HEK^{XBP1s} cells (*SI Appendix*, Table S1), again in agreement with the observation of decreased bisecting N-glycans by lectin microarrays (Fig. 2*A*).

Collectively, these data reveal that XBP1s activation in HEK^{XBP1s} cells substantially remodeled the composition of the membrane N-glycome, as summarized in Fig. 2*C* and *SI Appendix*, Table S2. Moreover, XBP1s-induced changes in the N-glycome were consistently detected both via lectin microarrays and MS. In particular, we observed a strong reduction in sialylation, specifically α2,6-sialylation, as well as a reduction in bisecting N-glycans.

Next, to ask whether induction of ER protein misfolding, and therefore all UPR pathways, has related effects on N-glycome composition, we performed the same analyses on membrane N-glycans from Tg-treated HEK^{XBP1s} cells. We found that the overall glycomic profile closely mirrored that of selective XBP1s activation in that we observed reduced sialylation and a reduction in bisecting GlcNAc (Dataset S3*A*). However, the magnitude of the changes was less substantial. SNA-I and diCBM40 still showed statistically significant decreases in binding (19 and 40%, respectively; Fig. 2*A* and *SI Appendix*, Fig. S3*A*, *Right*). In contrast, while other α2,6-sialic acid-binding lectins (e.g., PSL and TJA-I) also displayed reduced overall binding, they did not meet the statistical cutoff. A reduction in sialylation was also observed in the MALDI-TOF MS data, evident both in the relative abundance of sialylated to undecorated triantennary N-glycans (green peaks in Fig. 2*B*, *Top* versus Fig. 2*B*, *Bottom*) and the relative abundance of sialylated to undecorated tetraantennary N-glycans (red peaks in Fig. 2*B*, *Top* versus Fig. 2*B*, *Bottom*). Sialylation of biantennary N-glycans also decreased substantially upon Tg treatment (*SI Appendix*, Fig. S3*C*, *Left* versus *SI Appendix*, Fig. S3*C*, *Right*). GC-MS linkage analysis

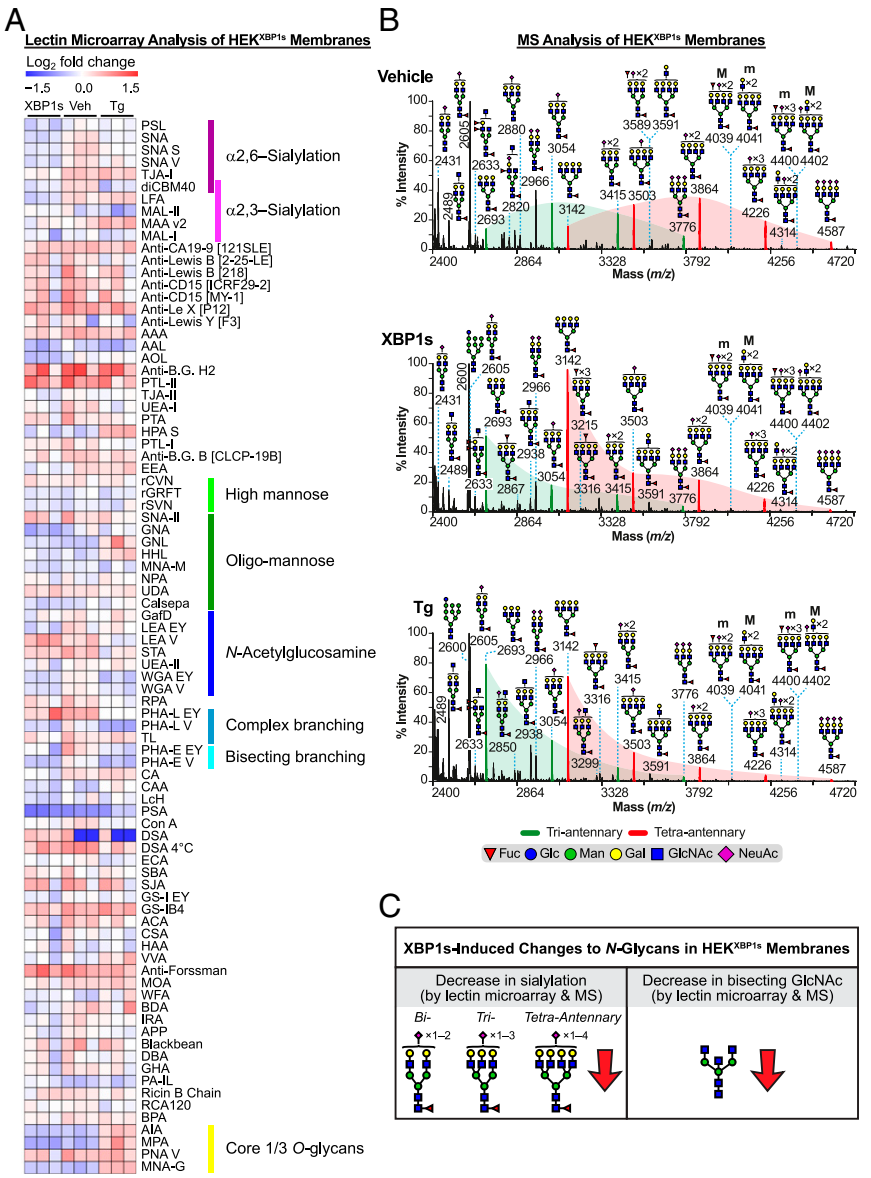

Fig. 2. Analysis of the HEK^{XBP1s} membrane glycoproteome. (*A*) Heatmap of lectin microarray data generated from HEK^{XBP1s} membrane glycoproteomes. Full lectin names, print concentration, and sources are listed in Dataset S2*A*. Color intensity represents normalized $\log_2$ ratio data relative to a pooled sample reference. Each column represents one biological replicate of the indicated sample. Select lectin groups with shared binding specificities are annotated (*Right*). See also *SI Appendix*, Fig. S3*A* and Dataset S3*A*. (*B*) Partial MALDI-TOF mass spectra from the HEK^{XBP1s} membrane proteome. Green and red peaks correspond to tri- and tetraantennary N-glycans with various levels of sialylation. Green- and red-shaded areas highlight the distribution shift of sialylation toward fewer NeuAcs on tri- and tetraantennary N-glycans. Structures above a bracket were not unequivocally defined. "M" and "m" designations indicate major and minor abundances, respectively. Putative structures are based on composition, tandem MS, and knowledge of biosynthetic pathways. All molecular ions are $[M+Na]^+$. High-mass spectra are presented in *SI Appendix*, Fig. S3*B*, with GC-MS data in *SI Appendix*, Table S1. (*C*) Summary of XBP1s-induced changes to the HEK^{XBP1s} membrane N-glycome (see also *SI Appendix*, Tables S2 and S3).

(*SI Appendix*, Table S1) confirmed a decrease in α2,6-linked NeuAcs, evidenced by a shift in the relative abundance of 6-linked galactose from 23.6% on vehicle-treated HEK^{XBP1s} cells to 4.1% on Tg-treated cells. Like XBP1s, activation of global ER stress by Tg also caused a loss of bisecting GlcNAc, observed by reduced PHA-E binding in lectin microarrays (Fig. 2*A* and *SI Appendix*, Fig. S3*A*, *Right*) and by a decrease in 3,4,6-mannose by GC-MS analysis (*SI Appendix*, Table S1). Notably, a gain in core 1/3 O-glycans was also observed upon Tg treatment, evidenced by increased binding to the lectins AIA, MPA, and MNA-G (Fig. 2*A* and *SI Appendix*, Fig. S3*A*, *Right*). Detailed O-glycan analysis was not performed using MALDI-TOF MS here, but this last result suggests that further investigation may reveal interesting ER stress-mediated changes to O-linked glycoforms, in addition to N-linked glycoforms. The Tg-mediated alterations in the HEK^{XBP1s} membrane glycome are summarized in *SI Appendix*, Table S3.

XBP1s Remodels HeLa^{XBP1s} Membrane N-Glycoproteomes in a Cell Type-Dependent Manner. We next asked whether activation of the XBP1s transcription factor has broader consequences for N-glycome composition across cell types. In particular, because cells derived from different tissues often have very different baseline N-glycome profiles (23, 24), we were interested in the consequences of XBP1s activation in distinctive cellular contexts. To address this question, we employed our HeLa^{XBP1s} cells following the workflow in Fig. 1*A*. We first confirmed that the baseline glycome profiles of HEK^{XBP1s} versus HeLa^{XBP1s} cells were different. By lectin microarray analysis, HEK^{XBP1s} and

HeLa^{XBP1s} cells displayed strikingly different levels of oligomannose N-glycans (Man_7 to Man_5) and sialylation epitopes (*SI Appendix*, Fig. S4). Additionally, we found using MALDI-TOF/TOF MS/MS that, whereas high-mass poly-LacNAc N-glycans in HEK^{XBP1s} membranes consisted of linear LacNAc repeats (*SI Appendix*, Fig. S3*D*), in HeLa^{XBP1s} cell membranes the high-mass N-glycans consisted of I-branched poly-LacNAc repeats (*SI Appendix*, Fig. S5 *A* and *B*). GC-MS linkage analysis confirmed the presence of 3,6-linked galactose in HeLa^{XBP1s} cells, in concordance with the presence of I-branched LacNAcs (*SI Appendix*, Table S1).

Coincident with these quite distinctive baseline N-glycome profiles, lectin microarray analysis revealed a unique shift in the membrane glycomic profile upon XBP1s activation in HeLa^{XBP1s} cells (Fig. 3*A*, *SI Appendix*, Fig. S5*C*, and Dataset S3*B*) relative to that observed in HEK^{XBP1s} cells. XBP1s-activated HeLa^{XBP1s} membranes exhibited increased levels of less processed N-linked glycans relative to vehicle-treated controls, based on increased signal from several high- (Man_9 to Man_7) and oligomannose-binding lectins (rGRFT, HHL, NPA, GNL, and Calsepa) (25). Additionally, XBP1s activation resulted in increased core fucosylation (PSA and LcH) and β1,6-GlcNAc branching (PHA-L, which binds tri- and tetraantennary glycans). No shift in sialylation was observed.

MALDI-TOF MS analysis was fully consistent with these observations. Similar to the microarray data, no significant changes in sialylation were observed. For example, the ratio of ions at *m/z* 3054, 3415, and 3776 (corresponding to triantennary N-glycans with one to three NeuAc residues, respectively) over the ion at *m/z* 2693 (corresponding to nonsialylated triantennary N-glycan) did not shift upon XBP1s activation (comparing the intensity of the green peaks within the green-shaded areas in Fig. 3*B*, *Top* versus Fig. 3*B*, *Middle*). Similarly, no change was observed in sialylation of the tetraantennary N-glycans (comparing the intensity of the red peaks within the red-shaded areas in Fig. 3*B*, *Top* versus Fig. 3*B*, *Middle*). Instead, consistent with the lectin microarrays, the most striking consequence of XBP1s activation for the HeLa^{XBP1s} membrane glycome was a 97% increase in the relative abundance of tetra- versus triantennary N-glycans (intensity of all of the red versus all of the green peaks in Fig. 3*B*, *Top* versus Fig. 3*B*, *Middle*). GC-MS linkage analysis further confirmed the MALDI-TOF MS and microarray data, demonstrating (*i*) an increase in tetraantennary N-glycans revealed by increased 2,4- and 2,6-linked mannose in the partially permethylated alditol acetates (*SI Appendix*, Table S1) and (*ii*) an increase in core fucosylation revealed by increased levels of 4,6-linked GlcNAc (*SI Appendix*, Table S1).

As performed here, MALDI-TOF MS does not permit quantitation of relative high- and oligomannose levels between two samples, and so we were unable to further validate that particular finding from the lectin microarray using the MS data. Moreover, the experimental strategy of cell-membrane isolation by ultracentrifugation can be problematic when assessing changes in levels of less processed N-glycans on membrane proteins, as all cell membranes are isolated in the ultracentrifugation step. Therefore, to further evaluate the increase in high-mannose levels observed via lectin microarrays upon XBP1s activation (Fig. 3*A*), we turned to a lectin-based flow cytometry approach (26). We incubated live HeLa^{XBP1s} cells, treated with dox or vehicle as above, with biotinylated HHL, a lectin that preferentially binds high-mannose N-glycans (27). We then stained cells with Cy5-streptavidin to enable quantitative fluorescence detection of high-mannose N-glycans. XBP1s-activated HeLa^{XBP1s} cells displayed a modest but significant increase in HHL signal compared with vehicle-treated control cells (*SI Appendix*, Fig. S6*A*, *Left* and *Middle*). We confirmed that HHL was detecting bona fide high-mannose N-glycans by showing that (*i*) inhibiting lectin binding with methyl α-D-mannopyranoside reduced the signal (*SI Appendix*, Fig. S6*A*, *Right*) and (*ii*) the mannosidase I inhibitor 1-deoxymannojirimycin (28) increased HHL binding without causing a loss of cell viability (*SI Appendix*, Fig. S6 *B–D*).

Collectively, these data reveal that XBP1s activation in HeLa^{XBP1s} cells substantially remodels the HeLa membrane N-glycome, as summarized in Fig. 3*C* and *SI Appendix*, Table S2. In particular, we observed strong increases in both core fucosylation and the abundance of tetraantennary N-glycans via both lectin microarray and MALDI-TOF MS analyses. In addition, the combination of lectin microarrays and lectin flow cytometry experiments revealed that XBP1s activation increased levels of high- and oligomannose N-glycans on the HeLa^{XBP1s} cell surface.

Stress-induced, global UPR activation via Tg treatment of HeLa^{XBP1s} cells also caused increases in high-mannose levels (Fig. 3*A* and *SI Appendix*, Fig. S5*C*, *Right*; see also Dataset S3*B*), demonstrated by significantly increased binding of the α1,2-mannose–specific antiviral lectins rSVN and rCVN, in addition to rGRFT. However, Tg treatment also induced a loss of β1,6-branched N-glycans based on decreased signal from PHA-L, revealing a distinct difference from the XBP1s-induced signal (Fig. 3*A* and *SI Appendix*, Fig. S5*C*, *Right*). Again, no changes in sialylation were observed. These observations were fully confirmed by our MALDI-TOF MS analysis, in which Tg-treated cells did not display increased tetraantennary N-glycans relative to vehicle-treated cells (red versus green shading in Fig. 3*B*, *Top* versus Fig. 3*B*, *Bottom*). Instead, as anticipated from the lectin microarray work (Fig. 3*A*), a decrease in 2,4- and 2,6-linked mannose was observed by GC-MS, the latter being consistent with a loss of β1,6-branched N-glycans (*SI Appendix*, Table S1). The Tg-mediated alterations in the HeLa^{XBP1s} membrane glycome are summarized in *SI Appendix*, Table S3.

In summary, the ability of XBP1s (or even stress-induced UPR activation) to globally remodel the N-glycome extends beyond just a single cell type. The molecular nature of the resulting changes in N-glycan distribution patterns is cell type-dependent, likely owing at least in part to differences in baseline N-glycome composition. The magnitude of the effects can be quite substantial.

XBP1s Remodels the N-Glycan Composition of the HEK^{XBP1s} Secretome. The observation that XBP1s activation alters the structure distribution pattern of N-glycans on cell surfaces in a cell type-dependent manner suggests that cell–cell interactions, cell adhesion, and receptor signaling could all be modified by XBP1s. Beyond cell membranes, a large portion of the N-glycoproteome is composed of soluble, secreted proteins. Alterations in the N-glycans on secreted proteins could provide a mechanism for long-distance transmission of cell stress signals, or engender other important phenotypes. Therefore, we next asked whether XBP1s-mediated remodeling extends to the secreted N-glycome.

The secretome from XBP1s-activated HEK^{XBP1s} cells displayed substantial N-glycome remodeling when analyzed by lectin microarrays (Fig. 4*A*, *SI Appendix*, Fig. S7, *Left*, and Dataset S3*C*). A decrease in both β1,6 N-glycan branching (PHA-L) and bisecting GlcNAc (PHA-E) was observed, similar to our findings for the HEK^{XBP1s} membrane N-glycome. A modest (27%) but not statistically significant decrease in binding to α2,6-sialylation epitopes based on the lectins SNA-I and diCMB40 was also observed. These results were confirmed by our MALDI-TOF MS and GC-MS analyses (see below). We also observed a significant increase in binding to oligomannose-targeting lectins (HHL, UDA, NPA, Calsepa, and GNA).

MALDI-TOF MS analysis (Fig. 4*B*) revealed that N-glycans isolated from the secretome of HEK^{XBP1s} cells featured abundant core fucosylated bi- (purple peaks; *m/z* 2244, 2605, and 2966), tetra- (red peaks; *m/z* 3142, 3503, 3864, 4226, and 4587), and, to a lesser extent, triantennary (green peaks; *m/z* 2693, 3054, 3415, and 3776) N-glycans. Upon XBP1s activation, the tri- and tetraantennary, but not the biantennary, N-glycans exhibited reduced sialylation (Fig. 4*B*, *Top* versus Fig. 4*B*, *Middle*). For example, the relative abundance of molecular ions at *m/z* 3503, 3864, 4226, and 4587 compared with *m/z* 3142 was reduced from vehicle-treated levels in the XBP1s-activated secretome (red peaks in Fig. 4*B*, *Top* versus Fig. 4*B*, *Middle*). GC-MS analysis confirmed a small reduction in α2,6-sialylation overall (*SI Appendix*, Table S1; 6-linked galactose: vehicle 98.9% versus XBP1s 63.8%), consistent with our lectin microarray analysis. The decreases in bisected N-glycans and β1,6-branching observed by microarray were also confirmed by our

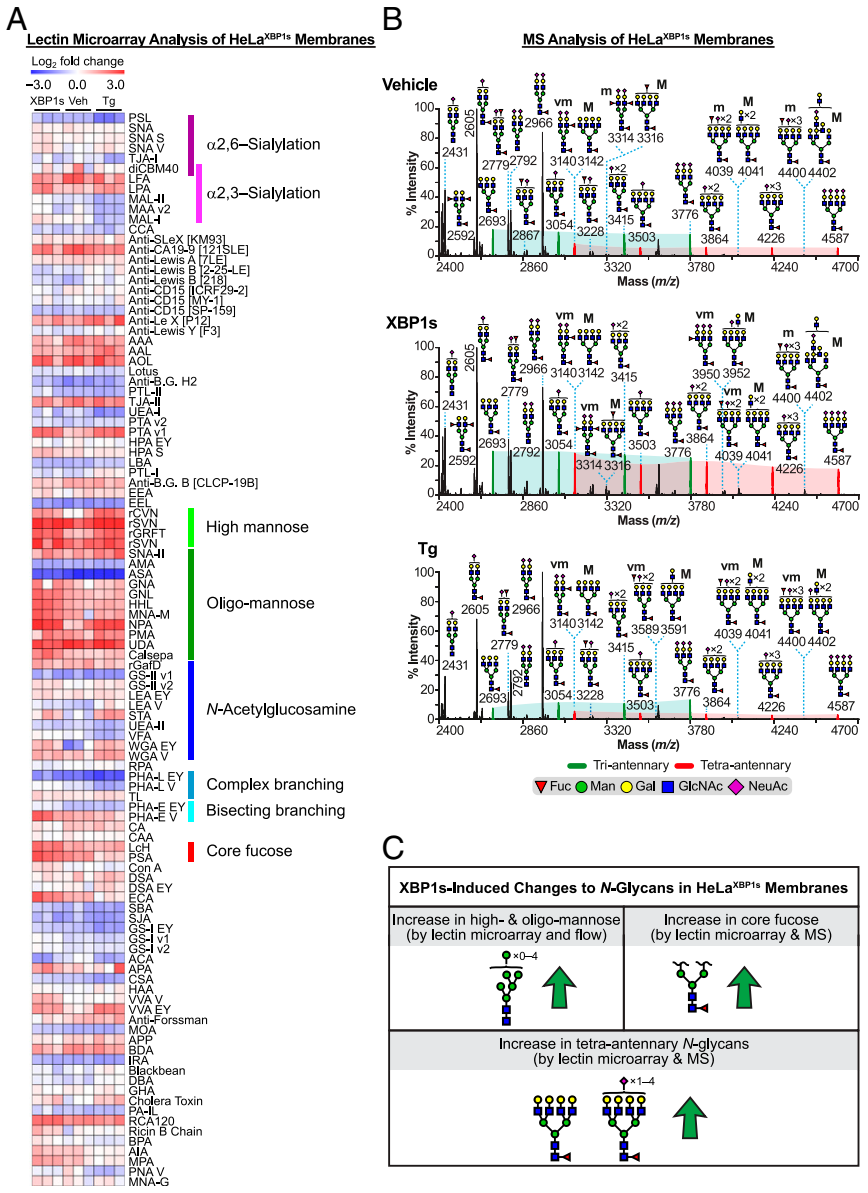

Fig. 3. Analysis of the HeLa^{XBP1s} membrane glycoproteome. (*A*) Heatmap of lectin microarray data generated from HeLa^{XBP1s} membrane glycoproteomes. Full lectin names, print concentration, and sources are listed in Dataset S2*B*. Color intensity represents normalized $\log_2$ ratio data relative to a pooled sample reference. Each column represents one biological replicate of the indicated sample. Select lectin groups with shared binding specificities are annotated (*Right*). See also *SI Appendix*, Fig. S5*C* and Dataset S3*B*. (*B*) Partial MALDI-TOF mass spectra from the HeLa^{XBP1s} membrane proteome. Green and red peaks correspond to tri- and tetraantennary N-glycans with various levels of sialylation. Green- and red-shaded areas highlight the increased abundance of tetraantennary N-glycans. The designation "vm" indicates very minor species; see Fig. 2*B* legend for description of other annotations. High-mass spectra and selected MS/MS fragmentations are presented in *SI Appendix*, Fig. S5 *A* and *B*, with GC-MS data in *SI Appendix*, Table S1. (*C*) Summary of XBP1s-induced changes to the HeLa^{XBP1s} membrane N-glycome (see also *SI Appendix*, Tables S2 and S3).

GC-MS data (*SI Appendix*, Table S1; 3,4,6-linked mannose: vehicle 4.7% versus XBP1s 2.3%; 2,6-linked mannose: vehicle 105.8% versus XBP1s 71.1%).

Collectively, these data reveal that XBP1s activation in HEK^{XBP1s} cells substantially remodels the composition of the secreted N-glycome, as summarized in Fig. 4*C* and *SI Appendix*, Table S2. Lectin microarray analyses revealed an increase in oligomannose levels. Both lectin microarray and MALDI-TOF MS analyses demonstrated a decrease in bisecting N-glycans. MALDI-TOF MS showed a loss of sialylation on specific N-glycan epitopes (for tri- and tetraantennary but not biantennary N-glycans), suggesting possible protein-specific effects influencing loss of sialylation. While the reduction in bisecting N-glycans and a loss of sialylation are both consistent with our observations for the HEK^{XBP1s} membrane N-glycomes (Fig. 2*C*), the increase in oligomannose levels is limited to the secretome. This observation highlights the importance of separately evaluating membrane and secreted N-glycans in glycomic experiments, as we have also noted in prior work (29, 30).

We also analyzed the consequences of stress-induced, global UPR activation via Tg treatment on the composition of the secreted N-glycome in HEK^{XBP1s} cells. The secreted N-glycome of Tg-treated HEK^{XBP1s} cells was similar to that of XBP1s-activated cells in that reduced levels of β1,6 N-glycan branching (decreased binding to PHA-L) and bisecting GlcNAc (decreased binding to PHA-E) were observed (Fig. 4*A* and *SI Appendix*, Fig. S7, *Right*; see also Dataset S3*C*). MALDI-TOF MS and GC-MS analyses (Fig. 4*B*, *Top* versus Fig. 4*B*, *Bottom* and *SI Appendix*, Table S1) confirmed the decreases in levels of tri- and tetraantennary N-glycans (β1,6 N-glycan branching shown by changes in 2,4-linked mannose and 2,6-linked mannose levels). There was no impact on overall α2,6-sialylation, although a decrease in α2,3-sialylation was observed via reduced binding to MAL-I, MAL-II, and diCBM40 (Fig. 4*A*). In contrast to the secretome of XBP1s-activated cells, Tg treatment did not induce an increase in oligomannose levels. These Tg-mediated alterations in the HEK^{XBP1s} secreted glycoproteome are summarized in *SI Appendix*, Table S3.

XBP1s Does Not Significantly Alter the Proteomic Composition of the HEK^{XBP1s} Secretome. We questioned whether XBP1s-driven changes in the N-glycan architecture of the HEK^{XBP1s} secretome could be attributed to changes in the composition of the proteome caused by XBP1s activation. To assess this hypothesis, we induced XBP1s by dox treatment for 24 h and then collected conditioned, serum-free DMEM after a 6-h incubation of vehicle-treated or

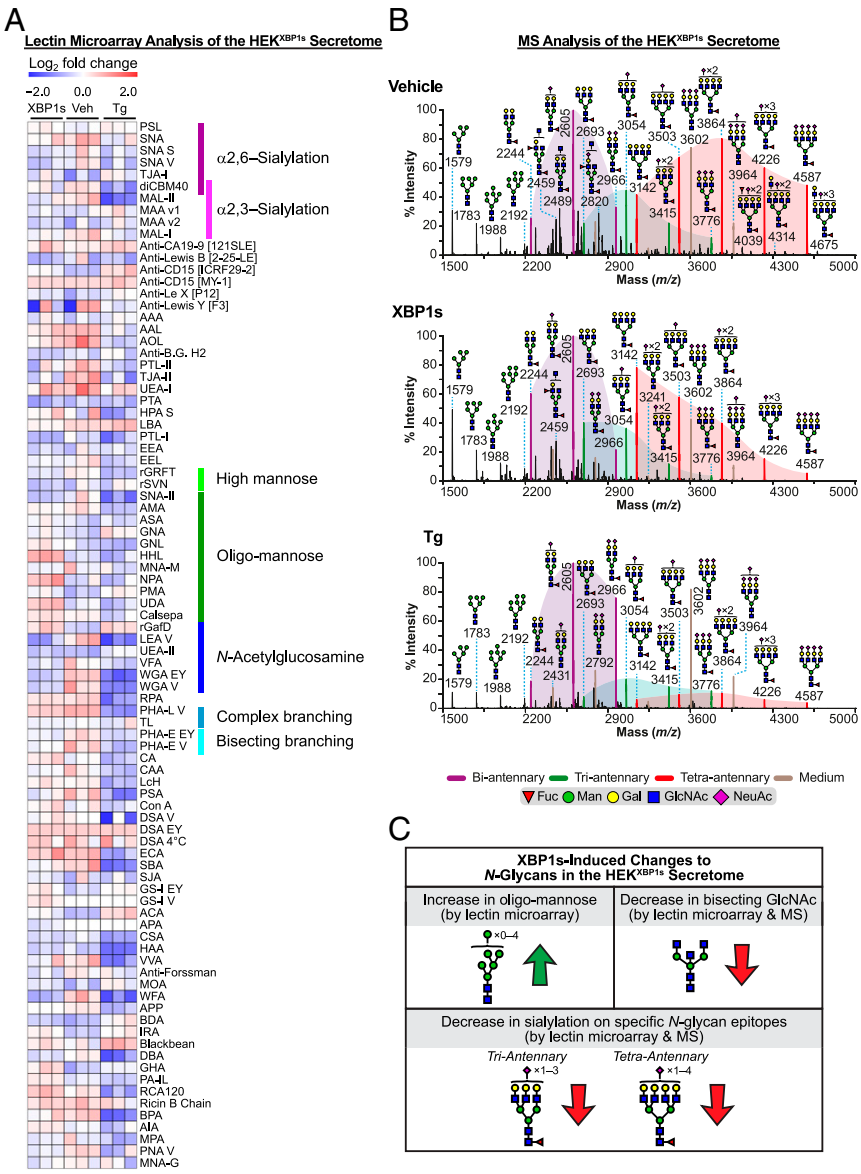

Fig. 4. Analysis of the HEK^{XBP1s} secreted glycoproteome. (*A*) Heatmap of lectin microarray data generated from HEK^{XBP1s} secreted glycoproteomes. Full lectin names, print concentration, and sources are listed in Dataset S2*A*. Color intensity represents normalized $\log_2$ ratio data relative to a pooled sample reference. Each column represents one biological replicate of the indicated sample. Select lectin groups with shared binding specificities are annotated (*Right*). See also *SI Appendix*, Fig. S7 and Dataset S3C. (*B*) Partial MALDI-TOF mass spectra from the HEK^{XBP1s} secretome. Purple, green, and red peaks correspond to bi, tri-, and tetraantennary N-glycans with various levels of sialylation. Purple-, green-, and red-shaded areas highlight the distribution shift of sialylation on the corresponding bi-, tri-, and tetraantennary N-glycans. Noncore fucosylated structures corresponded to residual FBS-derived N-glycans that we characterized previously (brown peaks; *m/z* 2792, 3602, and 3964) (52). These FBS-derived N-glycans were observed consistently in all samples and were excluded from the analyses as previously described (53). GC-MS data are presented in *SI Appendix*, Table S1. See Fig. 2*B* legend for description of other annotations. (*C*) Summary of XBP1s-induced changes to the HEK^{XBP1s} secreted N-glycome (see also *SI Appendix*, Tables S2 and S3).

dox-treated cells in biological triplicate. We used serum-free DMEM, not FreeStyle media optimized for HEK cell growth, because FreeStyle media contain various proprietary peptides that interfere with MS analysis. The use of serum-free DMEM limited us to a 6-h incubation instead of the longer incubation used in our glycomic experiments, to avoid extensive autophagy induction and cell toxicity. We precipitated total protein from the collected media, followed by denaturing, reducing, alkylating, and trypsinizing peptides. The digested samples were then labeled with isobaric mass tags to permit quantitative assessment of proteome composition and identify any XBP1s-mediated changes. Using this approach, we were able to quantify 700 secreted proteins across all samples (Dataset S4). Using significance thresholds of unadjusted *P* value ≤ 0.05 and fold change ≥ 1.5, we found that levels of only 16 of these 700 proteins were changed by XBP1s activation [we further note that no proteins qualified using a false discovery rate (FDR) threshold of 10% by Benjamini–Hochberg analysis]. Of those 16 proteins, only 9 are annotated in UniProtKB as being N-glycosylated. These data led us to conclude that the observed changes in the secreted glycome are unlikely to be driven by changes in the composition of the secreted proteome. Instead, we hypothesized that altered biosynthesis of N-glycans is the controlling factor.

Selective XBP1s Induction Remodels the Glycogene Transcriptome. Control mechanisms of N-glycan biosynthesis are not well-understood. One possible way in which induction of XBP1s could lead to an

CELL BIOLOGY

altered glycome is via enhanced flux through the secretory pathway that overwhelms the N-glycan maturation machinery and causes uncoordinated changes in structure distribution patterns. However, global changes in protein secretion that might suggest the Golgi N-glycan maturation pathway is overwhelmed upon XBP1s activation have not been detected [see Dataset S4 and work by Wiseman and coworkers (4)]. Moreover, while the changes in oligomannose levels in HeLa^{XBP1s} membranes and HEK^{XBP1s} secretomes could possibly be linked to increased flux overwhelming the N-glycan maturation pathway, it seems unlikely that many of the other changes observed (e.g., increases in core fucosylation, alterations in N-glycan branching, and changes in specific types of sialylation) could be explained by this hypothesis. Thus, although we cannot completely exclude the possibility, we believe the "overwhelming flux" hypothesis is unlikely to be correct.

A second possible explanation is that XBP1s activation either directly (as it is a transcription factor), or indirectly [as it can alter the expression of other transcription factors (4, 31, 32)] modifies the expression of enzymes involved in N-glycan maturation and biosynthesis (known as glycogenes), leading to transcriptionally encoded changes in N-glycome architecture. This explanation would be consistent with prior work showing that alterations in the expression of glycogene transcripts can induce changes in the N-glycome (24, 33). To evaluate this possibility, we used both previously published data for HEK^{XBP1s} cells (4) and our new RNA-sequencing (RNA-seq) data for HeLa^{XBP1s} cells to characterize the glycogene transcript-level changes induced by chronic, selective XBP1s activation in vehicle- versus dox-treated cells. In both HEK^{XBP1s} cells and HeLa^{XBP1s} cells, gene set enrichment analysis (GSEA) highlighted N-linked glycosylation as a highly enriched pathway under conditions of chronic, selective XBP1s activation (Dataset S1*C*) (4). Indeed, GO groups related to protein glycosylation are the most enriched gene sets in XBP1s-activated cells, after XBP1s- and IRE1-regulated aspects of the classical unfolded protein response. Furthermore, standard GSEA indicated strong enrichment of genes involved in biosynthesis of the lipid-linked oligosaccharide in both HEK^{XBP1s} and HeLa^{XBP1s} cells (*SI Appendix*, Fig. S8 and Dataset S1*E*). However, our data suggest that XBP1s activation does not globally alter transcripts involved in N-glycan maturation, as examination of a comprehensive gene set involved in N-glycan trimming and elaboration showed no global enrichment in XBP1s-activated cells (*SI Appendix*, Fig. S8 and Dataset S1*E*). This observation suggests that XBP1s regulates specific subsets of these glycogenes, consistent with the changes in levels of only specific epitopes observed in our glycomic analyses.

We next manually curated a list of 1,310 genes related to protein N-glycosylation from gene ontology datasets (the gene sets used and full list of N-glycosylation–related genes analyzed are shown in Dataset S5 *A* and *B*, respectively). These N-glycosylation–related genes included not just enzymes involved in N-glycan biosynthesis, trimming, and modification but also sugar transporters, monosaccharide synthases, and catabolic enzymes. We plotted the changes in expression levels of these individual glycogenes upon XBP1s activation for HEK^{XBP1s} and HeLa^{XBP1s} cells in the volcano plots in Fig. 5 *A* and *C*, respectively. As some glycogenes are expressed at low levels (34), we also employed a commercially available Qiagen RT^2 Profiler Human Glycosylation PCR Array to analyze transcript levels of selected glycogenes. For transcripts that were detected by multiple methods, we used the qPCR array results, rationalizing that the latter is more sensitive (35).

For HEK^{XBP1s} cells, 39 of 950 expressed glycogene transcripts were significantly altered by chronic XBP1s activation (teal in Fig. 5*A*; see Dataset S5*C* for a complete list of results). This analysis (*i*) confirms the remodeling of the glycogene transcriptome induced by XBP1s activation in HEK^{XBP1s} cells, especially for a number of glycogenes directly involved in N-glycan maturation, and (*ii*) is in concordance with key features of the N-glycome remodeling caused by XBP1s activation in both the membrane and secretome of HEK^{XBP1s} cells (Figs. 2*C* and 4*C*, respectively). Specifically (Fig. 5*B*), reduced levels of *MGAT3* (shown in pink in Fig. 5*A*), which encodes the enzyme responsible for introduction of bisecting GlcNAc residues (36), correlate with the reduction in bisected N-glycans observed most

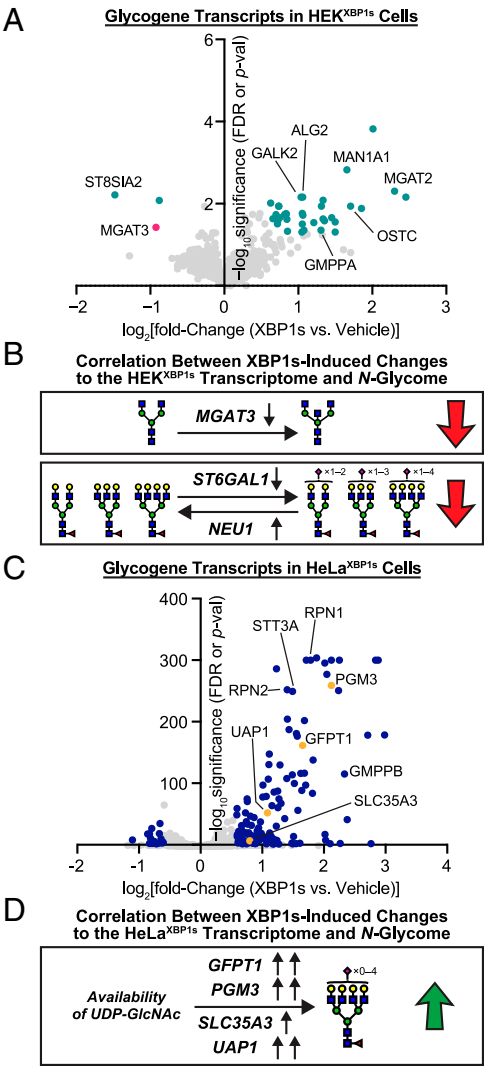

Fig. 5. Glycogene analysis in HEK^{XBP1s} and HeLa^{XBP1s} cells. (*A*) Volcano plot showing XBP1s activation-induced changes in glycosylation-related transcripts in HEK^{XBP1s} cells. Glycogenes analyzed are listed in Dataset S5*B*. Data shown were obtained either from the Qiagen Human Glycosylation qPCR Array or, if a transcript of interest was not included in the qPCR array, extracted from previously published HEK^{XBP1s} microarray data (4). Transcripts shown in teal meet significance and fold-change thresholds of FDR or *P* value ≤0.05 and fold change ≥1.5 upon XBP1s activation. Gene symbols are shown for outliers and transcripts of particular interest. (*B*) Decreased expression of *MGAT3* (shown in pink in *A*), a GlcNAc transferase (36), could account for the loss in bisecting GlcNAc observed on HEK^{XBP1s} secreted and membrane glycoproteins upon XBP1s activation. Decreased expression of *ST6GAL1* and increased expression of *NEU1* could account for the reduced sialylation observed for HEK^{XBP1s} secreted and membrane glycoproteins upon XBP1s activation. (*C*) Volcano plot showing XBP1s activation-induced changes in glycosylation-related transcripts in HeLa^{XBP1s} cells. Glycogenes analyzed are listed in Dataset S5*B*. Data shown were obtained either from the Qiagen Human Glycosylation qPCR Array or, if a transcript of interest was not included in the qPCR array, extracted from the RNA-seq data. Transcripts shown in blue meet significance and fold-change thresholds of FDR or *P* value ≤0.05 and fold change ≥1.5 upon XBP1s activation. Gene symbols are shown for outliers and transcripts of particular interest. (*D*) Increased expression of *GFPT1*, *PGM3*, *SLC35A3*, or *UAP1*, which are enzymes involved in regulating UDP-GlcNAc availability (shown in orange in *C*), could contribute to increased tetraantennary N-glycans observed on HeLa^{XBP1s} membranes upon XBP1s activation.

significantly in the HEK^{XBP1s} membrane N-glycome (Fig. 2*C*), but also in the secreted N-glycome (Fig. 4*C*). Although below the threshold for significance, there was also a decrease in the transcripts of the α2,6-sialyltransferase gene *ST6GAL1* (0.69-fold for XBP1s-activated HEK^{XBP1s} versus control, $P = 0.23$) and an increase in transcript levels for the sialidase gene *NEU1* (1.4-fold for XBP1s-activated HEK^{XBP1s} versus control, $P = 0.25$) that together may contribute to the loss of α2,6-sialylation, especially on more branched structures, that we observed (Fig. 5*B*).

For HeLa^{XBP1s} cells, 155 of 1,075 expressed glycogene transcripts were significantly altered by chronic XBP1s activation (blue in Fig. 5*C*; see Dataset S5*D* for a complete list of results). As was also the case in the HEK^{XBP1s} transcriptome data, this analysis is again in concordance with at least one key feature of the N-glycome remodeling caused by XBP1s activation in HeLa^{XBP1s} cell membranes (Fig. 3*C*). Specifically (Fig. 5*D*), XBP1s-activated HeLa^{XBP1s} cells exhibited increased expression of genes affecting nucleotide sugar availability (*SI Appendix*, Fig. S9 and Dataset S5*D*). Among the genes significantly overexpressed, we observed plasma membrane glucose transporters, such as GLUT1 and GLUT3 (encoded by *SLC2A1* and *SLC2A3*, respectively), which could potentially increase glucose availability in the cytosol. We also identified genes in the hexosamine biosynthetic pathway required for the biosynthesis of the UDP-GlcNAc sugar donor (37), including *PGM3* (4.35-fold increase), *UAP1* (2.12-fold increase), and the rate-limiting *GFPT1* (3.15-fold increase) (38). The increased expression of these enzymes, which collectively regulate cytosolic levels of UDP-GlcNAc (*SI Appendix*, Fig. S9), was accompanied by an increase in the Golgi UDP-GlcNAc transporter *SLC35A3*, thus increasing potential UDP-GlcNAc availability for Golgi glycosyltransferases (39). Levels of UDP-GlcNAc have been shown to affect the levels of tri- and tetraantennary N-glycans (37). It is therefore likely that, even in the absence of altered *MGAT5* expression, the abundance of tetraantennary N-glycans observed in HeLa^{XBP1s} cells might increase with XBP1s activation owing to increased UDP-GlcNAc concentrations in the Golgi. The connection between changes in UDP-GlcNAc levels and MGAT5-dependent β1,6-branching, in the absence of protein expression changes, is well-established (40). In further support of this hypothesis, changes in the level of functional *PGM3* have been correlated with altered N-glycomic profiles in human neutrophils (41), and increased expression of *UAP1* in human prostate cancer cells has been correlated with increased abundance of UDP-GlcNAc (42).

Collectively, these transcript-level results provide insights into the detailed mechanism of some of the XBP1s-induced changes in cellular N-glycome architectures. XBP1s activation results in a coordinated remodeling of the glycogene transcriptome at multiple levels, particularly for specific subsets of genes involved in N-glycan maturation and the availability of nucleotide sugar donors. In several cases, the alterations in glycogene transcript levels are in concordance with N-glycome–level changes induced by XBP1s activation. It should be noted, however, that N-glycosylation is regulated at many levels—not just transcriptionally, but also at the levels of translation (via microRNA), enzyme localization, and sugar metabolism/transport (13, 24, 34, 43–45). Thus, it is to be expected that XBP1s-induced changes in the glycogene transcriptome would be unlikely to directly explain all of the N-glycome changes we observed.

Discussion

Previous work has revealed the paradigmatic role of XBP1s in resolving protein misfolding stress and in expanding the secretory pathway. The impact of XBP1s activation on N-glycan maturation for specific ectopically overexpressed secreted proteins and possibly on N-glycan site occupancy has also been demonstrated (13, 18). However, it remained unclear whether or not selective XBP1s activation could alter N-glycan maturation on endogenous proteins. Strikingly, our data show that chronic XBP1s activation can generate changes of sufficient magnitude to be detected in glycome-wide assays that assess global carbohydrate composition in cell membranes and in the secretome.

XBP1s-mediated changes in N-glycome composition occur across multiple cell types. The nature of these changes displays some cell-type specificity, likely owing to the very different baseline N-glycome compositions of different cells. As summarized in *SI Appendix*, Table S2, upon stress-independent XBP1s activation in three different sets of samples, we observed increases in oligomannose levels in two sample sets (HEK^{XBP1s} secretomes and HeLa^{XBP1s} membranes), reductions in sialylation in two sample sets (HEK^{XBP1s} membranes and HEK^{XBP1s} secretomes), decreases in bisecting GlcNAc in two sample sets (HEK^{XBP1s} membranes and HEK^{XBP1s} secretomes), and increases in core fucosylation and tetraantennary N-glycans in one sample set (HeLa^{XBP1s} membranes). These results were consistently observed by multiple analytical methods, including lectin microarrays, MALDI-TOF MS, GC-MS, and lectin flow cytometry. We note that, in many cases, related changes were also induced by global, stress-mediated UPR activation using Tg treatment (*SI Appendix*, Table S3). However, the capacity of XBP1s activation alone to remodel the N-glycome indicates the key role of this transcription factor in driving N-glycome remodeling. ER stress is not required.

XBP1s-induced alterations in N-glycome architectures appear to reflect, at least in part, a coordinated response owing to remodeling of the glycogene transcriptome. In particular, changes in the expression of specific transcripts encoding enzymes directly involved in N-glycan maturation were induced by XBP1s activation. N-glycome remodeling driven by changes in glycogene transcript levels is consistent with observations that differential expression of glycosylation-related transcripts (24), or even individual glycogenes (46), can give rise to cell type- and disease-specific glycosylation profiles. However, full prediction of how glycogene transcriptome changes will be reflected in secreted and cell-membrane N-glycome architectures remains very challenging, likely owing to the fact that multiple variables, and not just glycogene transcript levels, play a role in N-glycan biosynthesis (13, 24, 34, 43–45). Thus, unsurprisingly, although some features of the XBP1s-remodeled N-glycome correlate with transcript-level changes in glycogene expression (Fig. 5 *B* and *D*), a direct correlation with all features does not exist. Further studies to fully detail the intermediate steps that propagate XBP1s activation to an altered N-glycome are an important subject for future work.

Another interesting aspect of our data is the differential impact of XBP1s activation on membrane versus secreted glycoproteins, particularly with respect to an increase in oligomannose levels in the secretome. Secreted glycoproteins on exosomes have been shown to have a glycosylation phenotype distinct from that of the originating cell membranes (29). Moreover, high- and oligomannose glycans are enriched in exosomes, and there are data indicating that glycosylation can act as a trafficking marker for these secreted vesicles (47). In the body, secreted glycoproteins can impact biology at sites distant to the cell, and there are many glycan-binding proteins involved in innate immunity. Cell-nonautonomous UPR signaling has been observed in metabolic regulation, immune system activation, and tumorigenesis (48), all processes that are also responsive to target- and/or epitope-specific glycosylation (17, 49, 50). Cumulatively, these observations raise the intriguing possibility that cells may use XBP1s-enacted changes in glycosylation in the secretome to signal for immune system functions or for cell-nonautonomous stress signaling (8, 10).

Selective activation of the IRE1-XBP1s arm of the UPR, even in the absence of ER protein misfolding stress, is a widely observed biological phenomenon. For example, selective XBP1s activation is involved in both memory formation and circadian clock regulation (9, 51). Similarly, selective induction of the XBP1s arm of the UPR plays a critical role in aspects of the immune response and in development (7, 8). The molecular mechanisms by which XBP1s activity influences these processes continue to be investigated. Our results indicate that a functional role for XBP1s-altered glycosylation must be considered. Beyond these phenomena, selective,

chronic XBP1s activation is also commonly observed in malignancies (11). It is noteworthy that another common feature of cancer cells is modified N-glycosylation (16, 50). Our findings open the possibility of a mechanistic connection between chronic XBP1s activity in cancer and metastasis-promoting, neoplastic N-glycosylation patterns.

In conclusion, the capacity of XBP1s-mediated transcriptional regulation to remodel the molecular architecture of the N-glycome provides a potential new pathway for intracellular stress signaling to be propagated to the extracellular milieu. XBP1s-induced changes to the N-glycome may also hold implications for pathologic processes, such as development of neoplastic glycosylation patterns that support cancer metastasis. In ongoing work, we are using glycoproteomic strategies to identify the specific endogenous proteins whose N-glycans are altered by XBP1s, and characterizing the functional consequences of such N-glycome remodeling.

Materials and Methods

Detailed protocols for the following procedures can be found in the *SI Appendix*: glycomic analyses by lectin microarray, MALDI-TOF MS, and TOF/TOF MS/MS; glycan linkage analysis by GC-MS; cell culture and reagents, RNA extraction, real-time qPCR, and RNA-seq; sample preparation for membrane proteomes and secretomes; lectin flow cytometry and metabolic assays; and secretome proteomic analysis.

ACKNOWLEDGMENTS. This work was supported by the 56th Edward Mallinckrodt Jr. Foundation Faculty Scholar Award, a Mizutani Foundation for Glycoscience Innovation Grant, an American Cancer Society–Ellison Foundation Research Scholar Award, and MIT (M.D.S.), NIH/NIAID Grant U01AI111598 (to L.K.M.), and BBSRC Grant BB/K016164/1 (to S.M.H. and A.D.). M.Y.W. was supported by a National Science Foundation Graduate Research Fellowship and a Prof. Amar G. Bose Research Grant. J.C.G. was supported by an NRSA from the NHLBI (F32-HL099245). This work was also supported in part by the NIH/NIEHS (Grant P30-ES002109) and Koch Institute Support (Core) Grant P30-CA14051 from the National Cancer Institute.

1. Wong MY, et al. (2018) Adapting secretory proteostasis and function through the unfolded protein response. *Curr Top Microbiol Immunol* 414:1–25.
2. Walter P, Ron D (2011) The unfolded protein response: From stress pathway to homeostatic regulation. *Science* 334:1081–1086.
3. Amin-Wetzel N, et al. (2017) A J-protein co-chaperone recruits BiP to monomerize IRE1 and repress the unfolded protein response. *Cell* 171:1625–1637.e13.
4. Shoulders MD, et al. (2013) Stress-independent activation of XBP1s and/or ATF6 reveals three functionally diverse ER proteostasis environments. *Cell Rep* 3:1279–1292.
5. Mendez AS, et al. (2015) Endoplasmic reticulum stress-independent activation of unfolded protein response kinases by a small molecule ATP-mimic. *eLife* 4:e05434.
6. Plate L, et al. (2016) Small molecule proteostasis regulators that reprogram the ER to reduce extracellular protein aggregation. *eLife* 5:e15550.
7. Martinon F, Chen X, Lee AH, Glimcher LH (2010) TLR activation of the transcription factor XBP1 regulates innate immune responses in macrophages. *Nat Immunol* 11:411–418.
8. Sun J, Liu Y, Aballay A (2012) Organismal regulation of XBP-1-mediated unfolded protein response during development and immune activation. *EMBO Rep* 13:855–860.
9. Martínez G, et al. (2016) Regulation of memory formation by the transcription factor XBP1. *Cell Rep* 14:1382–1394.
10. Taylor RC, Dillin A (2013) XBP-1 is a cell-nonautonomous regulator of stress resistance and longevity. *Cell* 153:1435–1447.
11. Chen X, et al. (2014) XBP1 promotes triple-negative breast cancer by controlling the HIF1α pathway. *Nature* 508:103–107.
12. Ruiz-Canada C, Kelleher DJ, Gilmore R (2009) Cotranslational and posttranslational N-glycosylation of polypeptides by distinct mammalian OST isoforms. *Cell* 136:272–283.
13. Wang ZV, et al. (2014) Spliced X-box binding protein 1 couples the unfolded protein response to hexosamine biosynthetic pathway. *Cell* 156:1179–1192.
14. Moremen KW, Tiemeyer M, Nairn AV (2012) Vertebrate protein glycosylation: Diversity, synthesis and function. *Nat Rev Mol Cell Biol* 13:448–462.
15. Zandberg WF, Kumarasamy J, Pinto BM, Vocadlo DJ (2012) Metabolic inhibition of sialyl-Lewis X biosynthesis by 5-thiofucose remodels the cell surface and impairs selectin-mediated cell adhesion. *J Biol Chem* 287:40021–40030.
16. Stowell SR, Ju T, Cummings RD (2015) Protein glycosylation in cancer. *Annu Rev Pathol* 10:473–510.
17. Pang PC, et al. (2009) Analysis of the human seminal plasma glycome reveals the presence of immunomodulatory carbohydrate functional groups. *J Proteome Res* 8:4906–4915.
18. Dewal MB, et al. (2015) XBP1s links the unfolded protein response to the molecular architecture of mature N-glycans. *Chem Biol* 22:1301–1312.
19. Lee A-H, Iwakoshi NN, Glimcher LH (2003) XBP-1 regulates a subset of endoplasmic reticulum resident chaperone genes in the unfolded protein response. *Mol Cell Biol* 23:7448–7459.
20. Lee AS (2014) Glucose-regulated proteins in cancer: Molecular mechanisms and therapeutic potential. *Nat Rev Cancer* 14:263–276.
21. Pilobello KT, Slawek DE, Mahal LK (2007) A ratiometric lectin microarray approach to analysis of the dynamic mammalian glycome. *Proc Natl Acad Sci USA* 104:11534–11539.
22. Ribeiro JP, et al. (2016) Characterization of a high-affinity sialic acid-specific CBM40 from *Clostridium perfringens* and engineering of a divalent form. *Biochem J* 473:2109–2118.
23. Fujitani N, et al. (2013) Total cellular glycomics allows characterizing cells and streamlining the discovery process for cellular biomarkers. *Proc Natl Acad Sci USA* 110:2105–2110.
24. Agrawal P, et al. (2014) Mapping posttranscriptional regulation of the human glycome uncovers microRNA defining the glycocode. *Proc Natl Acad Sci USA* 111:4338–4343.
25. Mori T, et al. (2005) Isolation and characterization of Griffithsin, a novel HIV-inactivating protein, from the red alga *Griffithsia* sp. *J Biol Chem* 280:9345–9353.
26. Moriwaki K, Miyoshi E (2014) Basic procedures for lectin flow cytometry. *Methods in Molecular Biology*, ed Hirabayashi J (Humana, New York), Vol 1200, pp 147–152.
27. Kaku H, Van Damme EJM, Peumans WJ, Goldstein IJ (1990) Carbohydrate-binding specificity of the daffodil (Narcissus pseudonarcissus) and amaryllis (Hippeastrum hybr.) bulb lectins. *Arch Biochem Biophys* 279:298–304.
28. Mendoza L, Olaso E, Anasagasti MJ, Fuentes AM, Vidal-Vanaclocha F (1998) Mannose receptor-mediated endothelial cell activation contributes to B16 melanoma cell adhesion and metastasis in liver. *J Cell Physiol* 174:322–330.
29. Batista BS, Eng WS, Pilobello KT, Hendricks-Muñoz KD, Mahal LK (2011) Identification of a conserved glycan signature for microvesicles. *J Proteome Res* 10:4624–4633.
30. Morrison CJ, et al. (2000) Modification of a recombinant GPI-anchored metalloproteinase for secretion alters the protein glycosylation. *Biotechnol Bioeng* 68:407–421.
31. Acosta-Alvear D, et al. (2007) XBP1 controls diverse cell type- and condition-specific transcriptional regulatory networks. *Mol Cell* 27:53–66.
32. Dong L, et al. (2011) Ets-1 mediates upregulation of Mcl-1 downstream of XBP-1 in human melanoma cells upon ER stress. *Oncogene* 30:3716–3726.
33. Chen HL, Li CF, Grigorian A, Tian W, Demetriou M (2009) T cell receptor signaling co-regulates multiple Golgi genes to enhance N-glycan branching. *J Biol Chem* 284:32454–32461.
34. Nairn AV, et al. (2008) Regulation of glycan structures in animal tissues: Transcript profiling of glycan-related genes. *J Biol Chem* 283:17298–17313.
35. Comelli EM, et al. (2006) A focused microarray approach to functional glycomics: Transcriptional regulation of the glycome. *Glycobiology* 16:117–131.
36. Narasimhan S (1982) Control of glycoprotein synthesis. UDP-GlcNAc:glycopeptide beta 4-N-acetylglucosaminyltransferase III, an enzyme in hen oviduct which adds GlcNAc in beta 1-4 linkage to the beta-linked mannose of the trimannosyl core of N-glycosyl oligosaccharides. *J Biol Chem* 257:10235–10242.
37. Dennis JW, Nabi IR, Demetriou M (2009) Metabolism, cell surface organization, and disease. *Cell* 139:1229–1241.
38. Broschat KO, et al. (2002) Kinetic characterization of human glutamine-fructose-6-phosphate amidotransferase I: Potent feedback inhibition by glucosamine 6-phosphate. *J Biol Chem* 277:14764–14770.
39. Maszczak-Seneczko D, et al. (2013) UDP-N-acetylglucosamine transporter (SLC35A3) regulates biosynthesis of highly branched N-glycans and keratan sulfate. *J Biol Chem* 288:21850–21860.
40. Lau KS, et al. (2007) Complex N-glycan number and degree of branching cooperate to regulate cell proliferation and differentiation. *Cell* 129:123–134.
41. Sassi A, et al. (2014) Hypomorphic homozygous mutations in phosphoglucomutase 3 (PGM3) impair immunity and increase serum IgE levels. *J Allergy Clin Immunol* 133:1410–1419.e13.
42. Itkonen HM, et al. (2015) UAP1 is overexpressed in prostate cancer and is protective against inhibitors of N-linked glycosylation. *Oncogene* 34:3744–3750.
43. Denzel MS, et al. (2014) Hexosamine pathway metabolites enhance protein quality control and prolong life. *Cell* 156:1167–1178.
44. Neelamegham S, Mahal LK (2016) Multi-level regulation of cellular glycosylation: From genes to transcript to enzyme to structure. *Curr Opin Struct Biol* 40:145–152.
45. Nairn AV, et al. (2012) Regulation of glycan structures in murine embryonic stem cells: Combined transcript profiling of glycan-related genes and glycan structural analysis. *J Biol Chem* 287:37835–37856.
46. Ohtsubo K, Chen MZ, Olefsky JM, Marth JD (2011) Pathway to diabetes through attenuation of pancreatic beta cell glycosylation and glucose transport. *Nat Med* 17:1067–1075.
47. Liang Y, et al. (2014) Complex N-linked glycans serve as a determinant for exosome/microvesicle cargo recruitment. *J Biol Chem* 289:32526–32537.
48. Imanikia S, Sheng M, Taylor RC (2018) Cell non-autonomous UPR(ER) signaling. *Curr Top Microbiol Immunol* 414:27–43.
49. Wellen KE, et al. (2010) The hexosamine biosynthetic pathway couples growth factor-induced glutamine uptake to glucose metabolism. *Genes Dev* 24:2784–2799.
50. Gaziel-Sovran A, et al. (2011) miR-30b/30d regulation of GalNAc transferases enhances invasion and immunosuppression during metastasis. *Cancer Cell* 20:104–118.
51. Zhu B, et al. (2017) A cell-autonomous mammalian 12 hr clock coordinates metabolic and stress rhythms. *Cell Metab* 25:1305–1319.e9.
52. Monk CR, Sutton-Smith M, Dell A, Garden OA (2006) Preparation of CD25(+) and CD25(−) CD4(+) T cells for glycomic analysis–A cautionary tale of serum glycoprotein sequestration. *Glycobiology* 16:11G–13G.
53. Chen Q, et al. (2015) Global N-linked glycosylation is not significantly impaired in myoblasts in congenital myasthenic syndromes caused by defective glutamine-fructose-6-phosphate transaminase 1 (GFPT1). *Biomolecules* 5:2758–2781.